

SAM3D: Zero-Shot 3D Object Detection via Segment Anything Model

Dingyuan Zhang¹, Dingkang Liang¹, Hongcheng Yang¹,
Zhikang Zou², Xiaoqing Ye², Zhe Liu¹, Xiang Bai¹

¹Huazhong University of Science and Technology, Wuhan, China

²Baidu Inc., China

<https://github.com/DYZhang09/SAM3D>

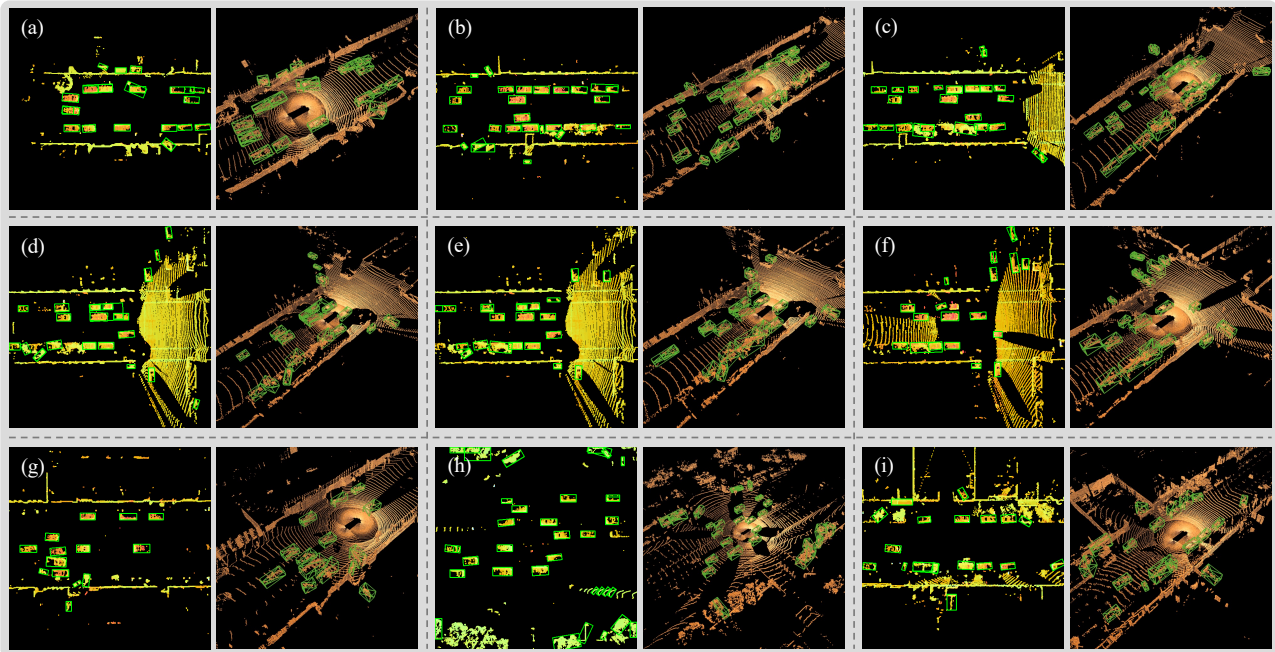


Figure 1: The visualizations of results from SAM3D. Each sub-figure corresponds to a single frame. Left side are visualizations of 2D bounding boxes under the Bird’s Eye View (BEV) and right side are of 3D bounding boxes.

Abstract

With the development of large language models, many remarkable linguistic systems like ChatGPT have thrived and achieved astonishing success on many tasks, showing the incredible power of foundation models. In the spirit of unleashing the capability of foundation models on vision tasks, the Segment Anything Model (SAM), a vision foundation model for image segmentation, has been proposed recently and presents strong zero-shot ability on many downstream 2D tasks. However, whether SAM can be adapted to 3D vision tasks has yet to be explored, especially 3D object detection. With this inspiration, we explore adapting the zero-shot ability of SAM to 3D object detection in

this paper. We propose a SAM-powered BEV processing pipeline to detect objects and get promising results on the large-scale Waymo open dataset. As an early attempt, our method takes a step toward 3D object detection with vision foundation models and presents the opportunity to unleash their power on 3D vision tasks.

1. Introduction

In the past few years, foundation models [1] have thrived and achieved great success on linguistic [18, 19, 2] and visual tasks [17, 13, 20], showing astonishing zero-shot and few-shot capabilities. Their advances encourage researchers and industries to extend the boundaries of what

artificial intelligence can do and have shown some fantastic products (e.g., ChatGPT [2] and Midjourney [16]) with the potential to change the world.

Recently, Kirillov *et al.* [14] proposed a new vision foundation model for image segmentation, the Segment Anything Model (SAM), trained on a huge dataset called SA-1B. The flexible prompting support, ambiguity awareness, and vast training data endow the SAM with powerful generalization, enabling the ability to solve downstream segmentation problems using prompt engineering. Some following works leverage the excellent zero-shot capability of SAM to solve other 2D vision tasks (e.g., medical image processing [27, 6, 9] and camouflaged object segmentation [25, 11, 12]). Although SAM presents great power on some 2D vision tasks, whether it can be adapted to 3D vision tasks still needs to be discovered. With this inspiration, a few works attempt to combine SAM with pre-trained 3D models to learn 3D scene representation (e.g., SA3D [3]) and single-view reconstruction (e.g., anything-3D [21]), showing promising results.

3D object detection, one of the fundamental tasks in 3D vision, has a wide range of real-world applications (e.g., autonomous driving). Although there are plenty of works [26, 15, 23, 22, 28] aim to solve this task, the zero-shot setting on 3D object detection is barely explored. Thus, considering the advance of SAM, it is natural to question: *Can we adapt the zero-shot capability of SAM to 3D object detection?* Note that although 3D-Box-Segment-Anything [4] also utilizes SAM for 3D object detection, it still relies on a pre-trained 3D detector VoxelNeXt [5] and mainly for interactive 3D detection and labeling.

In this paper, we aim to explore the zero-shot 3D object detection with SAM [14] alone. Considering SAM is initially built for 2D images, we need to represent a 3D scene into a 2D image carrying crucial 3D information (e.g., depths). Thus, the Bird’s Eye View (BEV) is a natural choice. With this observation, we present SAM3D, which uses SAM to segment on BEV maps and predicts objects based on the masks from its outputs.

We evaluate our method on the large-scale Waymo Open Dataset [24], and the results show the great potential of SAM on 3D object detection. Although this paper is only an early attempt and is still in progress, it gives a positive signal for applying vision foundation models like SAM for 3D vision, especially for 3D object detection.

2. Method

2.1. Preliminaries

Problem definition. We explore the zero-shot 3D object detection, in which we have a model F pre-trained on a labeled source dataset $D_s = \{X_i^s, Y_i^s\}$ and one 3D detection dataset $D_t = \{X_i^t\}$ without any annotation, where X^s, Y^s

are the input data and annotations of the source dataset respectively, and X^t is the input of the target dataset (point cloud in this paper). The goal of the zero-shot 3D object detection task is to maximize the performance of F on D_t without access to 3D annotations.

Revisit of SAM. Segment Anything Model (SAM) [14], which supports flexible prompts, interactive use, and ambiguity-aware outputs, has shown great zero-shot ability on many downstream segmentation tasks. Despite its capability, the design is surprisingly simple: a powerful image encoder computes an image embedding, a prompt encoder embeds prompts, and a lightweight mask decoder that combines information and predicts segmentation masks.

More specifically, for the image encoder, it uses a MAE [8] pre-trained Vision Transformer (ViT [7]) to extract image embedding. For the prompt encoder, it represents points and boxes by positional encodings and free-form text with an off-the-shelf text encoder from CLIP [17], and the mask prompts are embedded using convolutions and summed element-wise with the image embedding. The mask decoder employs a Transformer decoder (with prompt self-attention and cross-attention in two directions) followed by a dynamic mask head, which computes the mask foreground probability at each image location.

2.2. Overall framework

We consider point cloud as the input of our method, which is a 3D representation and naturally sparse, while SAM is trained for 2D images with dense semantics. Our basic idea is to translate LiDAR points into a 2D image-like representation with 3D information that narrows the domain gap, thus BEV is a straightforward choice.

We build the whole pipeline with SAM based on BEV, shown as Fig. 2. Our method mainly contains five steps:

- LiDAR-to-BEV projection translates LiDAR signals to BEV images. At this step, we use the projection equations to determine each point’s coordinate on the image plane and a predefined intensity-to-RGB mapping to get RGB vectors for pixels in a BEV image, making it more discriminative during processing.
- BEV post-processing modifies original BEV images with a simple operation. This step helps form more suitable inputs for SAM, leading to easier segmentation and better performance.
- SAM takes in modified BEV images and mesh grid prompts to segment foreground objects in BEV. In order to accelerate the segmentation process, we prune the prompts in this step without performance sacrifice.
- Mask post-processing filters noisy masks according to some rules drawn from priors, which reduces the number of false positives.

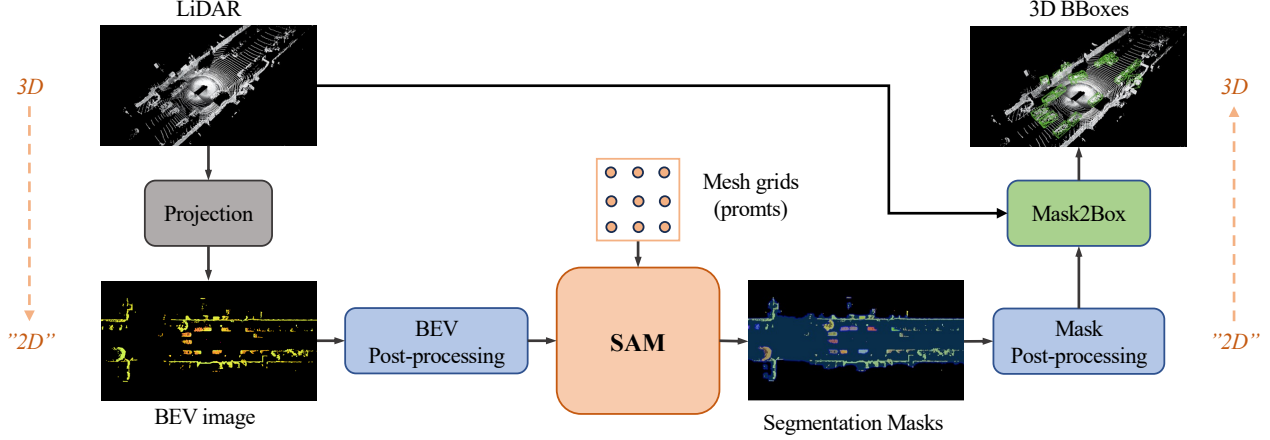


Figure 2: The overall framework of our method. We first project LiDAR points to colorful BEV images via a predefined palette, then post-process BEV images to better fit the requirements of SAM. After the segmentation, we post-process the noisy masks and finally predict 3D bounding boxes with the aid of LiDAR points.

- Mask2Box finds the minimum bounding boxes of foreground masks to extract 2D boxes in BEV and then interacts with LiDAR points, predicting the final 3D bounding boxes of objects.

In the following sections, we will describe the detailed designs for each step.

2.3. LiDAR-to-BEV projection

The duty of LiDAR-to-BEV projection is to translate N_p LiDAR points $P = \{(x_i, y_i, z_i)\}_{i=1}^{N_p}$ with range $L_x \leq x_i \leq U_x, L_y \leq y_i \leq U_y$ to a single BEV image $I \in \mathbb{R}^{H \times W \times 3}$.

Each point will fall into a grid of BEV image, and the position of grid (cx, cy) is calculated as follow:

$$cx_i = \lfloor (U_x - x_i) / s_x \rfloor, \quad (1)$$

$$cy_i = \lfloor (U_y - y_i) / s_y \rfloor, \quad (2)$$

where s_x, s_y are the pillar size of x and y axes, U_x, U_y are the coordinate upper bounds of x and y axes respectively, and $\lfloor \cdot \rfloor$ means the floor function.

After obtaining the positions of grids, we need to get the values filled into the BEV image. In order to make segmentation easier, we want the BEV image to be discriminative.

One finding is that the reflection intensity of points is useful, which means we can utilize the intensity $R = \{r_i\}_{i=1}^{N_p}$ to form the feature vectors of grids in a BEV image. Concretely, we first regularize the intensity to $[0, 1]$, and then take it to select color vectors from a predefined palette, which can be formally written as:

$$\mathbf{c}_i = \text{Palette}(\text{Norm}(r_i)) \in \mathbb{R}^3, \quad (3)$$

$$I[cx_i, cy_i, :] = \mathbf{c}_i, \quad (4)$$

where $\text{Palette} : \mathbb{R} \rightarrow \mathbb{R}^3$ is the predefined palette used for translating an intensity scalar to an RGB vector.

For those grids without projected points, we simply fill in all zero vectors, after which we get a discriminative BEV image $I \in \mathbb{R}^{H \times W \times 3}$.

2.4. BEV post-processing

Since SAM is trained on natural images, which contain "dense" signals and differ from the "sparse" BEV images, we need to post-process BEV images to narrow the gap. We use the morphology dilation in this paper, which can be interpreted as a max pooling, shown as Eq. 5.

$$I' = \text{MaxPool2D}(I), \quad (5)$$

where I' is the BEV image after post-processing.

2.5. Segmentation with SAM

Now we segment the BEV image using SAM, which supports various prompts like point, box, and mask prompts. Our goal in this step is to segment foreground objects as many as possible, so we choose to cover the whole image with mesh grid prompts. Specifically, we create 32×32 mesh grids evenly distributed on the image plane and regard them as point prompts to SAM.

Although this can cover the whole image, it is inefficient due to the natural sparsity of BEV images, with many prompts falling into empty space. Based on this observation, we prune the prompts. In particular, we project these prompts onto the BEV image, check the neighbor area of each prompt, and then discard prompts with no activated pixels around. This operation accelerates the whole pipeline dramatically, bringing 5× speed up (from 0.4 FPS to 2 FPS, on a single NVIDIA GeForce RTX 4090).

At the end of this step, we now get N_m segmentation masks $M = \{m_i \in \mathbb{R}^{H \times W}\}_{i=1}^{N_m}$ from SAM.

2.6. Mask post-processing

Despite SAM’s powerful zero-shot capability, a non-negligible domain gap still exists. Hence, the masks from SAM are noisy and need further processing.

In scenes of autonomous driving, typical cars have certain areas and aspect ratios, which can be used to filter out some false positives in masks M . In detail, we filter segmentation masks using an area threshold $[T_l^a, T_h^a]$ and an aspect ratio threshold $[T_l^r, T_h^r]$.

With these operations, we finally obtain N_o relative high-quality foreground masks $M' = \{m_i \in \mathbb{R}^{H \times W}\}_{i=1}^{N_o}$, each mask corresponds to a foreground object.

2.7. Mask2Box

After the segmentation, we need to predict 3D bounding boxes B^{3D} from the foreground masks M' . Since BEV images already carry depth information, we can directly estimate the horizontal attributes (*i.e.*, horizontal object center, length, width, and heading) of 3D bounding boxes from the 2D masks. While for the vertical attributes (*i.e.*, vertical object center and height), LiDAR points will be utilized as extra information compensation.

More specifically, we define the 3D bounding boxes as:

$$B^{3D} = \{(x_i^{3D}, y_i^{3D}, z_i^{3D}, dx_i^{3D}, dy_i^{3D}, dz_i^{3D}, \theta_i^{3D})\}_{i=1}^{N_o}, \quad (6)$$

where $(x_i^{3D}, y_i^{3D}, z_i^{3D})$, $(dx_i^{3D}, dy_i^{3D}, dz_i^{3D})$, and θ_i^{3D} are the 3D center, dimension, and orientation of the i -th object, respectively. N_o is the number of objects.

We first extract the 2D minimum bounding boxes from masks, defined as Eq. 7.

$$B^{2D} = \{(x_i^{2D}, y_i^{2D}, dx_i^{2D}, dy_i^{2D}, \theta_i^{2D})\}_{i=1}^{N_o}, \quad (7)$$

where (x_i^{2D}, y_i^{2D}) , (dx_i^{2D}, dy_i^{2D}) , and θ_i^{2D} are the 2D center, dimension, and rotate angle of the i -th object. N_o is the number of objects.

Then, we project these 2D attributes back to corresponding 3D attributes:

$$x_i^{3D} = U_x - (x_i^{2D} + 0.5) \times s_x, \quad (8)$$

$$y_i^{3D} = U_y - (y_i^{2D} + 0.5) \times s_y, \quad (9)$$

$$dx_i^{3D} = dx_i^{2D} \times s_x, \quad (10)$$

$$dy_i^{3D} = dy_i^{2D} \times s_y, \quad (11)$$

$$\theta_i^{3D} = \theta_i^{2D}, \quad (12)$$

where U_x, U_y are the point cloud ranges and s_x, s_y are the pillar size, defined in Sec. 2.3.

Finally, we estimate the vertical centers and heights with LiDAR points. The main idea is that we select points whose

BEV projections are inside the 2D bounding boxes and calculate the vertical attributes using their vertical coordinates, formally written as:

$$Z_i = \{z_j | (x_j, y_j, z_j) \text{ inside } B_i^{3D}\}, \quad (13)$$

$$dz_i^{3D} = \max(Z_i) - \min(Z_i), \quad (14)$$

$$z_i^{3D} = \min(Z_i) + \frac{dz_i^{3D}}{2}. \quad (15)$$

3. Experiments

3.1. Setup

Dataset. We evaluate our method on the Waymo Open Dataset [24], one of the large-scale datasets for autonomous driving. The dataset is split into 798 training sequences, 202 validation sequences, and 150 testing sequences. Since our method performs zero-shot object detection, we only focus on the validation sequences. For the metrics, because of the natural sparsity of point clouds and the lack of semantic label outputs, we only care about the mAP and mAPH of VEHICLE with a distance of at most 30 meters in this paper.

Hyperparameters. We set the point cloud range $L_x = L_y = -30.0m, U_x = U_y = 30.0m$ and the pillar size $s_x = s_y = 0.1m$. We use a 3×3 kernel for the dilation in BEV post-processing. For mask post-processing, we set the area thresholds $T_l^a = 200, T_h^a = 5000$ pixels, and the aspect ratio thresholds $T_l^r = 1.5, T_h^r = 4$, respectively. For SAM architecture, we use the default version (ViT-H) with pre-trained weights from its official repository.

3.2. Qualitative results

We first show the qualitative results of our method. Fig. 1 shows that relatively high-quality 2D rotated bounding boxes are generated from SAM outputs, indicating SAM’s great zero-capability. It means that SAM can generate good masks without touching BEV images and 3D annotations during training. With our mask post-processing and Mask2Box module, foreground masks can be translated into high-quality 3D bounding boxes.

Despite SAM’s incredible power, some obvious failure cases still exist: (1) SAM will generate duplicated masks when objects are close to each other. (2) Some background objects look similar to cars in BEV images, and SAM sometimes regards them as foregrounds by mistake. (3) Due to truncation, occlusion, and the sparsity of LiDAR signals, some cars are partially activated in BEV images, and thus SAM ignores these objects, leaving many false negatives.

3.3. Ablation study

We conduct ablation studies to figure out the contribution of different designs. For all experiments, we report the AP and APH only for VEHICLE in range [0, 30).

Table 1: The results of SAM3D when using different pillar sizes. We report metrics of VEHICLE in range [0,30) on Waymo *validation* set.

Pillar size $[s_x, s_y]$	Level1		Level2	
	AP	APH	AP	APH
$[0.05m, 0.05m]$	16.45	11.20	16.30	11.11
$[0.1m, 0.1m]$	19.51	13.30	19.05	12.98
$[0.2m, 0.2m]$	14.06	9.41	13.73	9.18
$[0.4m, 0.4m]$	~ 0	~ 0	~ 0	~ 0

Table 2: The results of SAM3D using different types of BEV images. We report metrics of VEHICLE in range [0,30) on Waymo *validation* set.

BEV type	Level1		Level2	
	AP	APH	AP	APH
Binary	0.94	0.55	0.92	0.53
Intensity	1.93	1.17	1.88	1.14
Intensity + Palette	19.51	13.30	19.05	12.98

Table 3: The results of SAM3D using different versions of SAM. We report metrics of VEHICLE in range [0,30) on Waymo *validation* set.

Architecture	Level1		Level2	
	AP	APH	AP	APH
ViT-B	17.30	11.58	16.90	11.31
ViT-L	19.94	13.25	19.48	12.93
ViT-H	19.51	13.30	19.05	12.98

Table 4: The ablations of post-processes. BEV post. means BEV post-processing. Area and Aspect ratio correspond to filter masks according to areas and aspect ratios in mask post-processing, respectively. We report metrics of VEHICLE in range [0,30) on Waymo *validation* set.

BEV post.	Area	Aspect ratio	Level1		Level2	
			AP	APH	AP	APH
-	✓	✓	11.01	7.68	10.93	7.64
✓	-	✓	17.52	11.93	17.11	11.65
✓	✓	-	14.05	9.61	13.72	9.38
✓	✓	✓	19.51	13.30	19.05	12.98

The effects of pillar size. According to Eq. 1, the pillar size will affect the resolution of BEV images, thus influencing the segmentation results of SAM. In this subsection, we evaluate the effects of pillar size, shown in Tab. 1. To make its effects more intuitive, we visualize the BEV under different pillar size settings in Fig. 3. When using larger pillar sizes such as $0.2m$ and $0.4m$, the discretization errors are relatively large, and it is hard to distinguish different objects

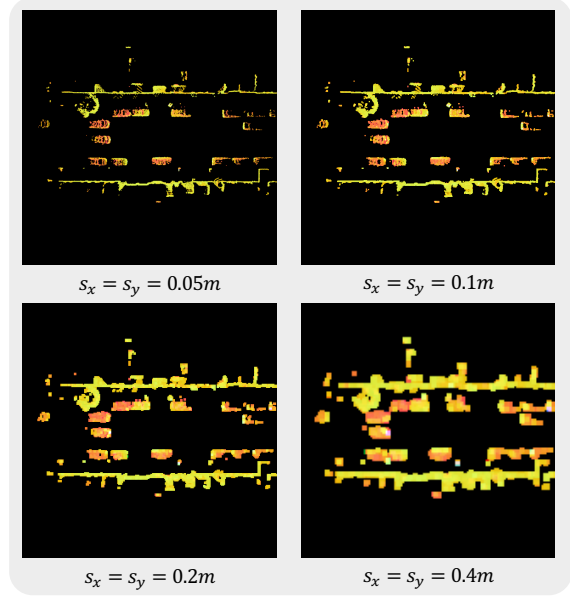


Figure 3: The visualization of BEV images under different pillar size settings.

when they are close to each other. However, too small pillar sizes also harm the performance. One possible reason is that due to the high resolution brought by small pillar size and the sparsity of LiDAR signals, it is difficult for individual instance to form a complete connected region, and SAM tends to separate one object into many parts. We set the pillar size as $0.1m$, which is a good balance.

The effects of reflection intensity. The way to project points into a BEV determines the visual appearance of BEV images, affecting the segmentation. In Sec. 2.3, we claim that using the reflection intensity of points and a predefined intensity-to-RGB mapping is helpful, and we evaluate its effects in this subsection. We compare our method with two other types: binary and intensity. For binary type, a pixel in a BEV image will be set to white if any point is projected into it, or it will be black otherwise. For intensity type, we use the normalized intensity as the grayscale. In Tab. 2, we can see that using intensity brings gains against the naive binary type, and mapping the intensity to rgb space further dramatically boosts the performance. Because the intensity and rgb mapping make BEV images more discriminative, SAM segments them more easily and precisely, thus improving the performance.

The effects of SAM architectures. Since SAM has different versions with different complexities, we conduct ablation studies to evaluate the effect of model complexity. Tab. 3 reveals that using SAM with less capacity performs worse. However, there is only a marginal difference between SAM with ViT-L and ViT-H. We argue that the model

capacity is not the performance bottleneck when using large models, and the power of SAM still needs to be fully unleashed. For insurance purposes, we use SAM with ViT-H.

The effects of BEV post-processing. In Sec. 2.4, we use the morphology dilation to post-process the BEV image for better segmentation. We conduct experiments to figure out its effect in this subsection, shown in the first row of Tab. 4. Without BEV post-processing, it drops about 8% AP and 5% APH on both Level 1 and Level 2. As we have claimed, BEV post-processing helps narrow the gap between BEV and natural images (training data of SAM), leading to better segmentation and detection results.

The effects of mask post-processing. In Sec. 2.6, we propose the mask area and aspect ratio thresholds $(T_l^a, T_h^a), (T_l^r, T_h^r)$ to filter noisy masks from SAM. We also conduct experiments to test its effect, shown in the second and third row of Tab. 4. Since there still exists a non-negligible domain gap and the masks from SAM are noisy, it is obvious that all operations in mask post-processing are essential. Dropping any of them will result in a significant performance decrease compared to the full model.

4. Discussion

Through the qualitative results and ablation studies, we show that it is possible to leverage SAM, trained on large-scale segmentation datasets without any 3D annotation, to solve the zero-shot object detection task for outdoor scenes.

However, there are some vital areas for improvement for our current method, and we leave these issues to be solved in the future:

- Utilizing BEV images as representations means our method may be unsuitable for indoor scenes. Finding a better scene representation will be a good solution.
- Due to the occlusion, truncation, and sparsity of LiDAR points, our method generates many false negatives, especially for distant objects. Considering the information from other modalities will be helpful.
- Although we have already reduced the inference time by $5\times$, the inference speed (2 FPS on a single NVIDIA GeForce RTX 4090) is still limited to the complexity of SAM, especially when the number of point prompts is large. Conducting model compression and distillation might solve this problem.
- Our method currently does not support multi-class detection because of the lack of semantic label outputs from SAM. One possible solution is to leverage 3D vision-language models (e.g., CLIP Goes 3D [10]) for zero-shot classification.

Although our method is only an early attempt, it shows the great possibility and opportunity to unleash the potential

of foundation models like SAM on 3D vision tasks, especially on 3D object detection. With technologies like few-shot learning and prompt engineering, we can take advantage of vision foundation models more effectively to better solve 3D tasks, especially considering the vast difference between scales of 2D and 3D data.

5. Conclusion

This paper explores the zero-shot 3D object detection with the visual foundation model SAM and proposes the SAM3D. To narrow the gap between the training data of SAM and 3D LiDAR signals, we use the BEV images to represent 3D outdoor scenes. We propose a SAM-powered BEV processing pipeline to utilize the great zero-shot capability of SAM for zero-shot 3D object detection. Qualitative and ablation experiments on Waymo open dataset show promising results for adapting the zero-shot ability of SAM to 3D object detection. Although this paper is only an early attempt, we believe it presents a possibility and opportunity to unleash the power of foundation models like SAM on 3D tasks with technologies like few-shot learning, model distillation, and prompt engineering in the future.

References

- [1] Rishi Bommasani, Drew A Hudson, Ehsan Adeli, Russ Altman, Simran Arora, Sydney von Arx, Michael S Bernstein, Jeannette Bohg, Antoine Bosselut, Emma Brunskill, et al. On the opportunities and risks of foundation models. *arXiv preprint arXiv:2108.07258*, 2021.
- [2] Tom Brown, Benjamin Mann, Nick Ryder, Melanie Subbiah, Jared D Kaplan, Prafulla Dhariwal, Arvind Neelakantan, Pranav Shyam, Girish Sastry, Amanda Askell, et al. Language models are few-shot learners. *Proc. of Advances in Neural Information Processing Systems*, 33:1877–1901, 2020.
- [3] Jiazhong Cen, Zanwei Zhou, Jiemin Fang, Wei Shen, Lingxi Xie, Xiaopeng Zhang, and Qi Tian. Segment anything in 3d with nerfs. *arXiv preprint arXiv:2304.12308*, 2023.
- [4] Yukang Chen, Jianhui Liu, Xiangyu Zhang, Xiaojuan Qi, and Jiaya Jia. 3d-box-segment-anything. <https://github.com/dvlab-research/3D-Box-Segment-Anything.git>, 2023.
- [5] Yukang Chen, Jianhui Liu, Xiangyu Zhang, Xiaojuan Qi, and Jiaya Jia. Voxelnext: Fully sparse voxelnet for 3d object detection and tracking. In *Proc. of IEEE Intl. Conf. on Computer Vision and Pattern Recognition*, 2023.
- [6] Ruining Deng, Can Cui, Quan Liu, Tianyuan Yao, Lucas Walker Remedios, Shunxing Bao, Bennett A Landman, Yucheng Tang, Lee E Wheless, Lori A Coburn, et al. Segment anything model (sam) for digital pathology: Assess zero-shot segmentation on whole slide imaging. In *Medical Imaging with Deep Learning, short paper track*, 2023.
- [7] Alexey Dosovitskiy, Lucas Beyer, Alexander Kolesnikov, Dirk Weissenborn, Xiaohua Zhai, Thomas Unterthiner,

- Mostafa Dehghani, Matthias Minderer, Georg Heigold, Sylvain Gelly, et al. An image is worth 16x16 words: Transformers for image recognition at scale. In *Proc. of Intl. Conf. on Learning Representations*, 2021.
- [8] Kaiming He, Xinlei Chen, Saining Xie, Yanghao Li, Piotr Dollár, and Ross Girshick. Masked autoencoders are scalable vision learners. In *Proc. of IEEE Intl. Conf. on Computer Vision and Pattern Recognition*, pages 16000–16009, 2022.
- [9] Sheng He, Rina Bao, Jingpeng Li, P Ellen Grant, and Yangming Ou. Accuracy of segment-anything model (sam) in medical image segmentation tasks. *arXiv preprint arXiv:2304.09324*, 2023.
- [10] Deepti Hegde, Jeya Maria Jose Valanarasu, and Vishal M Patel. Clip goes 3d: Leveraging prompt tuning for language grounded 3d recognition. *arXiv preprint arXiv:2303.11313*, 2023.
- [11] Ge-Peng Ji, Deng-Ping Fan, Peng Xu, Ming-Ming Cheng, Bowen Zhou, and Luc Van Gool. Sam struggles in concealed scenes—empirical study on “segment anything”. *arXiv preprint arXiv:2304.06022*, 2023.
- [12] Wei Ji, Jingjing Li, Qi Bi, Wenbo Li, and Li Cheng. Segment anything is not always perfect: An investigation of sam on different real-world applications. *arXiv preprint arXiv:2304.05750*, 2023.
- [13] Chao Jia, Yinfei Yang, Ye Xia, Yi-Ting Chen, Zarana Parekh, Hieu Pham, Quoc Le, Yun-Hsuan Sung, Zhen Li, and Tom Duerig. Scaling up visual and vision-language representation learning with noisy text supervision. In *Proc. of Intl. Conf. on Machine Learning*, pages 4904–4916. PMLR, 2021.
- [14] Alexander Kirillov, Eric Mintun, Nikhila Ravi, Hanzi Mao, Chloe Rolland, Laura Gustafson, Tete Xiao, Spencer Whitehead, Alexander C Berg, Wan-Yen Lo, et al. Segment anything. *arXiv preprint arXiv:2304.02643*, 2023.
- [15] Alex H Lang, Sourabh Vora, Holger Caesar, Lubing Zhou, Jiong Yang, and Oscar Beijbom. Pointpillars: Fast encoders for object detection from point clouds. In *Proc. of IEEE Intl. Conf. on Computer Vision and Pattern Recognition*, pages 12697–12705, 2019.
- [16] Midjourney. Midjourney. <https://www.midjourney.com>, 2022.
- [17] Alec Radford, Jong Wook Kim, Chris Hallacy, Aditya Ramesh, Gabriel Goh, Sandhini Agarwal, Girish Sastry, Amanda Askell, Pamela Mishkin, Jack Clark, et al. Learning transferable visual models from natural language supervision. In *Proc. of Intl. Conf. on Machine Learning*, pages 8748–8763. PMLR, 2021.
- [18] Alec Radford, Karthik Narasimhan, Tim Salimans, Ilya Sutskever, et al. Improving language understanding by generative pre-training. 2018.
- [19] Alec Radford, Jeffrey Wu, Rewon Child, David Luan, Dario Amodei, Ilya Sutskever, et al. Language models are unsupervised multitask learners. *OpenAI blog*, 1(8):9, 2019.
- [20] Aditya Ramesh, Mikhail Pavlov, Gabriel Goh, Scott Gray, Chelsea Voss, Alec Radford, Mark Chen, and Ilya Sutskever. Zero-shot text-to-image generation. In *Proc. of Intl. Conf. on Machine Learning*, pages 8821–8831. PMLR, 2021.
- [21] QiuHong Shen, Xingyi Yang, and Xinchao Wang. Anything-3d: Towards single-view anything reconstruction in the wild. *arXiv preprint arXiv:2304.10261*, 2023.
- [22] Shaoshuai Shi, Chaoxu Guo, Li Jiang, Zhe Wang, Jianping Shi, Xiaogang Wang, and Hongsheng Li. Pv-rcnn: Point-voxel feature set abstraction for 3d object detection. In *Proc. of IEEE Intl. Conf. on Computer Vision and Pattern Recognition*, pages 10529–10538, 2020.
- [23] Shaoshuai Shi, Xiaogang Wang, and Hongsheng Li. Point-rcnn: 3d object proposal generation and detection from point cloud. In *Proc. of IEEE Intl. Conf. on Computer Vision and Pattern Recognition*, pages 770–779, 2019.
- [24] Pei Sun, Henrik Kretzschmar, Xerxes Dotiwalla, Aurelien Chouard, Vijaysai Patnaik, Paul Tsui, James Guo, Yin Zhou, Yuning Chai, Benjamin Caine, et al. Scalability in perception for autonomous driving: Waymo open dataset. In *Proc. of IEEE Intl. Conf. on Computer Vision and Pattern Recognition*, pages 2446–2454, 2020.
- [25] Lv Tang, Haoke Xiao, and Bo Li. Can sam segment anything? when sam meets camouflaged object detection. *arXiv preprint arXiv:2304.04709*, 2023.
- [26] Yan Yan, Yuxing Mao, and Bo Li. Second: Sparsely embedded convolutional detection. *Sensors*, 18(10):3337, 2018.
- [27] Tao Zhou, Yizhe Zhang, Yi Zhou, Ye Wu, and Chen Gong. Can sam segment polyeps? *arXiv preprint arXiv:2304.07583*, 2023.
- [28] Yin Zhou and Oncel Tuzel. Voxnet: End-to-end learning for point cloud based 3d object detection. In *Proc. of IEEE Intl. Conf. on Computer Vision and Pattern Recognition*, pages 4490–4499, 2018.